

Article

# Transmission Strategy for Simultaneous Wireless Information and Power Transfer with a Non-Linear Rectifier Model

Ning Pan <sup>†</sup>, Mohammad Rajabi, Steven Claessens, Dominique Schreurs \*  and Sofie Pollin

Department of Electrical Engineering (ESAT), KU Leuven, B-3001 Leuven, Belgium; valen12134@126.com (N.P.); mohammad.rajabi@kuleuven.be (M.R.); steven.claessens@kuleuven.be (S.C.); sofie.pollin@kuleuven.be (S.P.)

\* Correspondence: dominique.schreurs@kuleuven.be; Tel.: +32-16-321821

<sup>†</sup> Current address: Huawei Technologies.

Received: 8 June 2020; Accepted: 29 June 2020; Published: 1 July 2020



**Abstract:** Most studies determining data rate or power conversion efficiency (PCE) of simultaneous wireless information and power transfer (SWIPT) focus on ideal models for the non-linear energy harvester, or focus on simplified waveforms that carry no information. In this paper, we study SWIPT using realistic waveforms and a measurement-based energy harvesting model. For a special class of multisine waveforms carrying only information in the phase, we analyze PCE as a function of waveform design, including the impact of pre-equalization to mitigate wireless channel distortion. A balanced pre-equalizer that trades off between the peak-to-average power ratio (PAPR) and signal to noise ratio, maximizing the total PCE is proposed. The impact on the information rate of the analyzed waveforms is also presented. The results show that balanced pre-equalizers can improve the total PCE more than three times within 5% rate loss compared to the pre-equalizer that solely maximizes the signal PAPR or the capacity using the same transmit power. We also show that the maximum normalized PCE is increased by a factor of two by only allowing phase modulation to ensure the PAPR of one symbol, compared to traditional modulation schemes that carry information in both phase and amplitude to maximize spectral efficiency.

**Keywords:** simultaneous wireless information and power transfer; non-linear rectifier; multi-tone signal; transmission strategy

## 1. Introduction

The concept of simultaneous wireless information and power transfer (SWIPT) has emerged as a potential scheme to realize the Internet-of-Things, consisting of many small devices. In SWIPT, the radio frequency (RF) source is used to carry both information and power [1]. However, a realistic SWIPT system is often restricted by the limited received power [2].

Previous research has shown that the RF to direct current (DC) power conversion efficiency (PCE) can be improved by using high peak-to-average power ratio (PAPR) waveforms such as multisine signals, which highlights the potential of using multisine signals in SWIPT systems. [3–6].

A considerable amount of studies have been published on the topic of transmission strategies for the MISO (Multiple Input Single Output) SWIPT system [7–10]. The authors of [7] designed optimal and sub-optimal joint beam-forming and power ratio splitting strategies for a multi-user MISO system with a quasi-static flat-fading channel. The work of [8] considered a more practical MISO SWIPT system where the channel state information is not perfect at the base station. Shi et al. [9] proposed a strategy to maximize energy efficiency of data transmission by jointly applying zero-forcing beam-forming and power splitting. Similarly, the researchers of [10] balanced the system fairness and

throughput by optimization of the beam-former and power splitter. However, all the aforementioned studies considered a linear wireless power transfer model. As the rectifier, which is the key component to transfer RF power to DC, is not linear, a more complex model is needed.

To design reliably a transmission strategy for a realistic SWIPT system, a non-linear energy harvesting model is necessary. While there exists several nonlinear energy harvesting models in literature [11–15], these models solely reveal the influence from the signal power or PAPR. Three such general energy harvesting models were compared in [16], showing that only the complete rectifier circuit model shows the complete influence of the received RF signal.

To evaluate the PCE corresponding to different multi-tone signal excitations, we adopt the complete circuit model in [17] to calculate the harvested DC power, thereby using the exact Shockley equation and other RF circuit parameters. This model is valid for a wide range of rectifiers and for different input power levels. While the complete circuit model makes the analytical derivation of the optimal transmission strategy not possible, it gives results that match the measurements well [17].

Several attempts have discussed the optimal input symbol distribution for information transfer for a given wireless power transfer constraint [18,19]. Moreover, several works have studied potential modulation schemes to improve the PCE in SWIPT systems [20–22]. These approaches adopt a simple nonlinear model for the rectifier and/or are based on amplitude modulation based techniques. In this work, we investigate the multisine phase-shift keying (PSK) modulation since this scheme would not distort the signal envelope and thus the PAPR, and this is combined with a realistic nonlinear rectifier model.

To evaluate the information rate of the signals, we rely on the capacity bound of PSK modulation as a function of obtained symbol energy to noise ratio. As a benchmark, we also consider quadrature amplitude modulation (QAM) which allows both amplitude and phase modulation. It is shown by simulations that the proposed multisine PSK scheme significantly improves the normalized PCE (defined as the harvested DC power divided by the transmitted power), however it decreases the information rate due to the loss of a degree of freedom in the modulation, as will be discussed next.

This paper studies the performance, including the impact of the frequency-selective wireless channel and the non-linear rectifier, of pre-equalizing strategies maximizing the SNR (signal to noise ratio) at the receiver, the PAPR of the received signal, and the channel capacity in a multisine signal based SWIPT system. The pre-equalizer maximizing the SNR boosts the received power of each tone; while the pre-equalizer maximizing PAPR ensures the rectifier operates at the highest PCE at the same input power level. It is shown that simply maximizing the SNR of each tone or PAPR is not the best strategy for SWIPT. A balanced pre-equalizer, trading-off between the SNR and PAPR of the received signal, is proposed to improve the normalized PCE as much as possible. In addition, we also compare our proposed transmission strategy to the low-complexity transmission strategy optimizing solely WPT as proposed in [23], and the water-filling strategy optimizing solely channel capacity. Besides, the transmission strategies are also evaluated considering the conventional QAM modulation.

The simulation and measurement results show that the normalized PCE can be improved up to a factor of 3 when using the optimal pre-equalizers with a channel capacity loss under 5% in the multisine PSK SWIPT system. On the other hand, the pre-equalizer proposed in [23] leads to the highest normalized PCE and the lowest capacity for the SWIPT system using QAM. Last but not least, it is shown that by applying the multisine PSK, the maximum normalized PCE is improved up to 60% compared to the one using QAM since the PAPR is improved.

The rest of the paper is organized as follows. Section 2 introduces the system model. In Section 3, we demonstrate the multisine PSK and QAM modulations, and the corresponding information rate. Section 4 addresses the considered non-linear energy harvesting model as well as the PCE dependency on the PAPR and power level of the received signals. Section 5 presents the derivation of the transmission strategies for multisine PSK and QAM modulations. Section 6 compares the normalized PCE and information rate of the multisine PSK and QAM modulations, applying the proposed transmission strategies. We conclude this paper in Section 7.

Notations: In this paper, we define the time domain signal using lower-case letters with time variation  $t$  as  $a(t)$ . Vectors are represented by lowercase boldface vectors.  $\|\cdot\|_1$  and  $\|\cdot\|$  denotes the Taxicab norm and the Euclidean norm, respectively. The sign  $\circ$  represents the element-wise Hadamard operation [24].

## 2. System Model

In this section, we introduce the system overview of the multisine signal based SWIPT, experiencing a frequency-selective fading channel.

### 2.1. System Overview

We are considering a single-link SWIPT system consisting of one single antenna source node and one user capable of decoding information and harvesting RF power simultaneously, as shown in Figure 1.

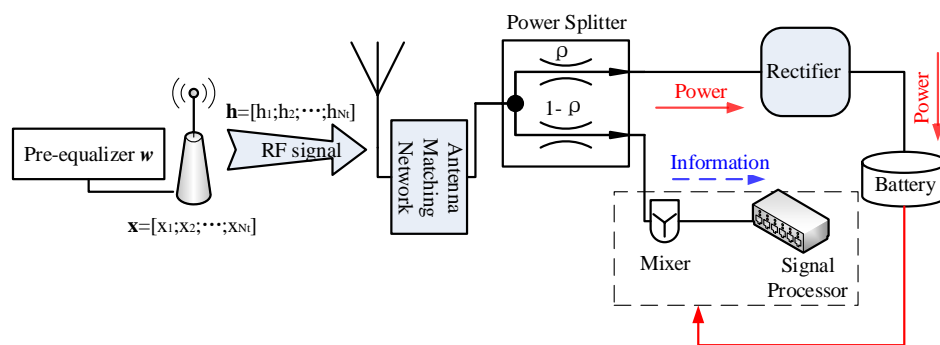


**Figure 1.** Multisine based simultaneous wireless information and power transfer (SWIPT) system overview.

The source node transmits multisine signals  $s(t)$  to the user through a frequency-selective channel  $h(t)$ . After reception by the antenna with adapted matching network, the signal is divided into two parts by the power splitter with power splitting ratio  $\rho$ . The  $\rho$  portion of the received signal power is converted to DC power by the rectifier. The DC power is then accumulated in the energy storage device, i.e., battery. The stored energy is used to supply power to the mixer and the signal processor. The remaining  $1 - \rho$  portion of the signal power is applied to the information decoder. In the information decoder, the received RF signal is first converted to baseband by the mixer. Then the baseband signal passes through the signal processor to recover the source information. After the ideal matched filtering in the processor, the information rate is bounded by the channel capacity. The power splitting factor  $\rho$  is considered to be a variable in this work.

### 2.2. Multisine Transmitted Signal

The source node transmits an  $N_t$ -tone multisine signal  $s(t)$  with bandwidth  $B$ . The tones are equally spread around center frequency  $f_c$  as  $f_n = f_c + \left(\frac{N_t-1}{2} + n - 1\right) \frac{B}{N_t}$ . The time-domain transmission signal  $s(t)$  is expressed as

$$s(t) = \Re \left[ \sum_{n=1}^{N_t} x_n e^{j2\pi f_n t} \right]. \tag{1}$$

with  $x_n(t) = a_n(t)e^{j\phi_n(t)}$  the  $n$ -th tone with amplitude  $a_n(t)$  and phase  $\phi_n(t)$ . As we assume block fading to simplify the notations, we will neglect the time index  $t$  in all channel and symbol notations that are constant over a multisine signal in the remainder. In this work, we will mainly focus on multisine PSK modulation, by which each tone has equal amplitude and phase in one symbol.

### 2.3. Pre-Equalization

To compensate the signal distortion caused by the wireless channel, we propose a channel adaptive pre-equalizer for SWIPT. This channel-adaptive pre-equalizer weighs the transmitted signal with a weight to optimize the SWIPT performance based on the perfect Channel State Information (CSI) at the transmitter, without changing the total transmit power. Therefore, we normalize the transmit power in this work. The received power, however, depends on the random channel fading. As we neglect path loss in our analysis, this means that we can instantaneously have a larger received power compared to the transmitted power, due to the diversity gain related to multipath. On average, transmitted and received power are the same. We assume  $\mathbf{w} = [w_1; w_2; \dots]$  is the general pre-equalizer, where  $w_n$  is a complex weight multiplied with the transmitted signal at frequency bin  $f_n$ .

### 2.4. Frequency-Selective Channel

After pre-equalization, the signal passes the frequency-selective Rayleigh fading channel. Hereby, we assume the channel is constant during the symbol period, thus a block fading channel. The channel between the source node and the user's antenna is denoted as  $\mathbf{h} = [h_1; h_2; \dots; h_{N_t}]$ , where  $h_n \sim \mathcal{CN}(0, 1)$  [25] and the channel white Gaussian noise is denoted as  $\mathbf{n} = [n_1; n_2; \dots; n_{N_t}]$ , where  $n_n \sim \mathcal{CN}(0, \sigma^2)$ ,  $\sigma^2$  is the noise power of  $n$ -th bin.

### 2.5. Signal at Receiver Antenna

Knowing the frequency domain response of the source signal as  $\mathbf{x} = [x_1; x_2; \dots; x_{N_t}]$ , the received signal is expressed as

$$\begin{aligned} y(t) &= \Re \left( \sum_{n=1}^{N_t} (h_n w_n x_n + n_n) e^{j2\pi f_n t} \right), \\ &= \Re \left( \sum_{n=1}^{N_t} (h_n w_n x_n + n_n) e^{j2\pi(f_c + m_n \Delta f)t} \right), \end{aligned} \tag{2}$$

with  $m_n = \left( \frac{N_t-1}{2} + n - 1 \right)$  and  $\Delta f = \frac{B}{N_t}$  the sub-carrier spacing. Then the signal complex response  $c_n$  is  $c_n = x_n w_n h_n$ . The instantaneous phase per tone  $\varphi_n(t)$  is time-varying depending on the carrier and can be written as

$$\varphi_n(t) = 2\pi m_n \Delta f t + \phi_n + \angle h_n + \angle w_n, \tag{3}$$

The instantaneous amplitude of each tone remains  $|c_n|$ , but the vector sum of tones varies over the symbol period. We can simplify  $y(t)$  to

$$y(t) = \Re \left( \sum_{n=1}^{N_t} \left( c_n e^{j\Theta_n(t)} + n_n e^{j\Theta_n(t)} \right) \right), \tag{4}$$

with  $\Theta_n(t) = 2\pi(f_c + m_n \Delta f)t$ .

To capture the PAPR of the received signal, we transform (2) into an equation of the envelope multiplied with the carrier wave. By applying Euler's formula [26], we can rewrite the received signal as a time-varying signal at a carrier frequency  $f_c$  as

$$y(t) = A(t) \cos(2\pi f_c t + \Psi(t)) + \sum_{n=1}^{N_t} n_n \cos(2\pi f_c t + m_n \Delta f), \tag{5}$$

where  $A(t)$  is the signal envelope which equals the amplitude of  $\sum_{n=1}^{N_t} c_n e^{j\Theta_n(t)}$  and  $\Psi(t)$  is the phase of  $\sum_{n=1}^{N_t} c_n e^{j\Theta_n(t)}$ . The time-varying envelope of the received signal is represented as

$$A(t) = \sqrt{\sum_{n=1}^{N_t} |c_n|^2 + \sum_{i \neq j} 2|c_i||c_j| \cos[\varphi_i(t) - \varphi_j(t)]} \leq \|\mathbf{c}\|_1, \quad (6)$$

The bottom equation holds if  $\varphi_i(t) - \varphi_j(t) = 0$ ,  $i \neq j$ . Since the noise is very small compared to the transmitted signal and therefore the noise influence on the PAPR of the received signal can be ignored,  $PAPR_r$  is bounded by

$$PAPR_r \leq \frac{2\|\mathbf{c}\|_1^2}{\|\mathbf{c}\|^2}. \quad (7)$$

The RF signal is then split by a power divider (Figure 1). The fraction  $(1 - \rho)$  of the RF signal goes into the information decoder assuming perfect matching and no distortion. Then signal to noise ratio (SNR) for each frequency bin is

$$\gamma_n = \frac{(1 - \rho) \frac{|c_n|^2}{2}}{(1 - \rho) \sigma^2 + \sigma_{\text{mixer}}^2}. \quad (8)$$

Hereby, the noise power at each bin  $\sigma^2 = \frac{kTB N_F}{N_t}$  is a function determined by thermal temperature  $T$ , signal bandwidth  $B$ , and noise figure  $N_F$ . The white Gaussian mixer noise is introduced after the power divider with variance  $\sigma_{\text{mixer}}^2$ . The other fraction  $\rho$  of the RF signal goes into the energy harvester, producing a DC output.

### 3. Information Rate

The channel capacity limits the data rate of reliable transmissions in the system, which is an important figure of merit for information transfer. While capacity depends on the channel itself, there are different capacity bounds for phase or amplitude modulation. In this paper, we compare the impact of phase and amplitude modulation of a multisine signal on capacity and information transfer. The considered modulation schemes, and their corresponding information rate, are discussed next.

#### 3.1. QAM Modulation

Firstly, we consider a popular modulation scheme allowing both amplitude and phase modulation for each sub-carrier as a baseline. This scheme is also known as QAM-OFDM (quadrature amplitude modulation–orthogonal frequency-division multiplexing). In this scheme, the source symbol  $x_n$  follows the complex normal distribution as  $x_n \sim \mathcal{CN}\left(0, \frac{P_t}{N_t}\right)$ .

Knowing the SNR of each frequency bin (8), the channel capacity implementing this scheme is then

$$C_{QAM} = \sum_{n=1}^{N_t} \int \frac{B}{N_t} \log_2(1 + \gamma_n) Pr(\gamma_n) d\gamma_n. \quad (9)$$

$Pr(\gamma_n)$  represents the probability that the SNR reaches the value  $\gamma_n$ .

#### 3.2. Multisine PSK Modulation

Secondly, we introduce the multisine PSK modulation scheme, which is the default modulation scheme considered in this work. In this scheme, the information is embedded in the phase  $\phi_n$  only. Specifically, to ensure the optimized waveform for wireless power transfer (WPT) [27], all tones have the same amplitude  $a = \sqrt{\frac{2P_t}{N_t}}$  and phase as  $\phi = \phi_n = \phi(t)$  in one symbol. Specifically,  $\phi(t)$  is fixed during one symbol period, which equals the multisine envelope period  $T_s = \frac{1}{\Delta f} = \frac{N_t}{B}$ , so that the information is modulated without changing the designed signal envelope.

Figure 2 shows two examples applying the multisine PSK modulation: First we show a binary PSK where  $\phi(t)$  alternates between 0 and  $\pi$ ; in the second example,  $\phi(t)$  follows a uniform distribution between 0 and  $2\pi$ . It is clear that both result in the same PAPR, only the location of the peak amplitude in the symbol period varies.

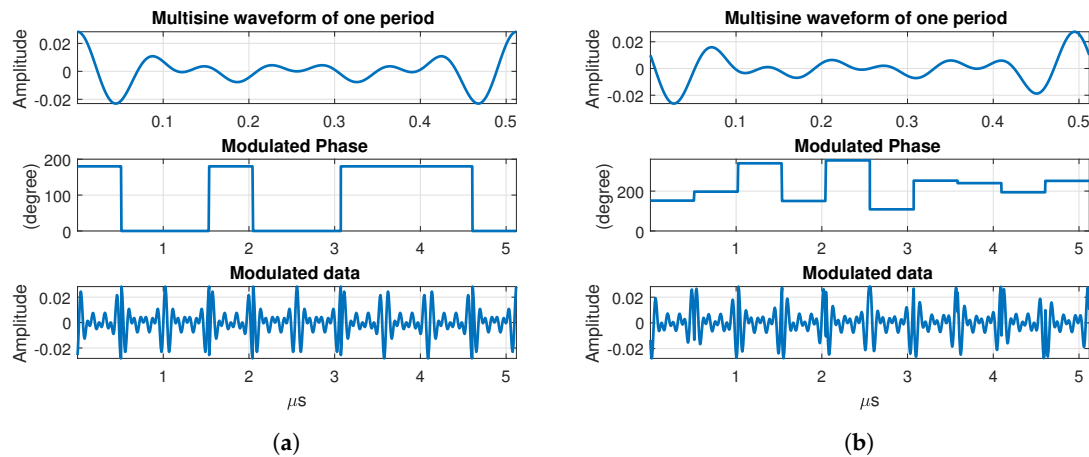


**Figure 2.** Four-tone multisine PSK modulation scheme (a)  $\phi(t) \in \{0, \pi\}$  and (b)  $\phi(t)$  selected randomly from uniform distribution  $[0, 2\pi]$ , with  $f_c = 10$  MHz and bandwidth  $BW = 10$  kHz.

By applying the same phase on each tone, a smaller bit error rate can be achieved at the cost of a lower bit rate. For example, considering M-PSK is applied, the bit rate is  $N_f \log_2 M$  for independent coding (as in OFDM) and  $\log_2 M$  is the bit error rate when considering joint coding. The bit error rate is  $Q\left(\frac{E_s}{N_f N_0 \log_2 M}\right)$  for independent coding and  $Q\left(\frac{E_s}{N_0 \log_2 M}\right)$  for joint coding, where  $N_0$  is the noise power spectral density. If  $M$  goes to infinity, the bit rate and bit error rate of independent coding and dependent coding converge. The bit rate of reliable transmissions is bounded by the total channel capacity experiencing the frequency-selective channel [25] and each sub-channel is bounded by the PSK channel capacity [28]. As the per tone coding strategy does not matter for very large  $M$ , and as capacity is the same for both, we use the capacity equation to evaluate the information transfer performance. Thus the channel capacity with multisine PSK modulation experiencing frequency-selective channel is

$$C_{PSK} = \sum_{n=1}^{N_f} \int \frac{1}{T_s} \log_2 \sqrt{\frac{4\pi}{e} \gamma_n} Pr(\gamma_n) d\gamma_n. \quad (10)$$

It should be noted that the maximum capacity is achieved when  $\phi(t)$  follows the uniform distribution  $[0, 2\pi]$  [28].

#### 4. PCE Dependency on PAPR and Power Level

In this section, the impact of PAPR and received signal power level on the PCE of the rectifier is presented by both simulations and measurements.

We derive the harvested DC power depending on the received signal using a circuit-based analysis [17], considering the basic rectifier scheme as in Figure 3. The basic rectifier consists of a rectifier matching network avoiding RF signal reflection, a rectifying diode as the main RF-DC transformer, and a low-pass RC filter to filter out the RF response and to control the ripple.

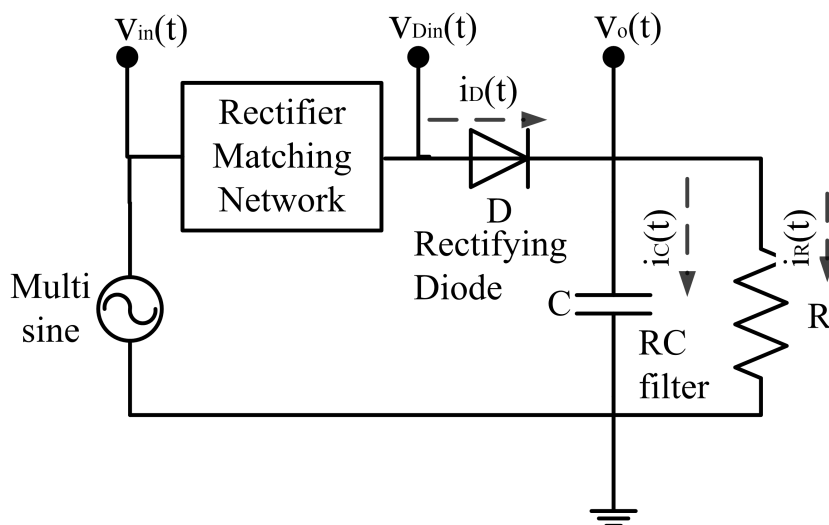


Figure 3. Basic rectifier scheme.

Since symbol rate and channel fading are slow compared to the circuit’s transient time needed for reaching a constant DC output, we consider constant channel coefficients and symbol during the considered time block. Knowing the received signal with power splitting coefficient  $\rho$  and the matched rectifier resistance  $R_{match}$ , we can compute the instantaneous voltage into the rectifier  $v_{in}(t)$  as [17]

$$v_{in}(t) = \Re \left[ \sum_{n=1}^{N_f} (h_n w_n x_n + n_n) e^{j2\pi f_n t} \right] \sqrt{\rho R_{match}}. \tag{11}$$

Following the matching network of the rectifier, the voltage seen from the diode to the end of the circuit is  $v_{D_{in}}(t)$ . Subsequently, we can derive the system model as:

$$v_D(t) = v_{D_{in}}(t) - v_o(t), \tag{12a}$$

$$i_D(t) = i_C(t) + i_R(t), \tag{12b}$$

$$i_D(t) = I_s \left( e^{\frac{v_D(t)}{nV_T}} - 1 \right), \tag{12c}$$

$$i_C(t) = C \frac{dv_o(t)}{dt}, \quad i_R(t) = \frac{v_o(t)}{R}, \tag{12d}$$

where  $v_D(t)$ ,  $v_{D_{in}}(t)$ ,  $v_o(t)$ ,  $i_D(t)$ ,  $i_C(t)$ ,  $i_R(t)$ ,  $I_s$ ,  $n$ ,  $V_T$  represent the voltage over the diode, instantaneous voltage into the diode, instantaneous voltage at the output of the diode, current flowing through the diode, current through the capacitor, current through the resistor, diode’s characteristic saturation current, ideality factor, and thermal voltage, respectively, as can be seen in Figure 3.

After proper transformation, the instantaneous output voltage is derived by solving the ordinary differential equation (ODE) function as below

$$\frac{dv_o(t)}{dt} = \frac{I_s}{C} \left( e^{\frac{v_{D_{in}}(t) - v_o(t)}{nV_T}} - 1 \right) - \frac{v_o(t)}{RC}. \tag{13}$$

Since the right hand side of Equation (13) is a complicated non-linear function, a unique analytical solution is impossible or very hard to achieve. Thus we propose to use an ODE solver to achieve the numerical solution.

Having obtained the instantaneous voltage in time domain, the output DC voltage  $V_{DC}$  is the mean value of the diode's output voltage  $v_o$  over a steady period as [17]

$$V_{DC} = \frac{1}{T - t_{steady}} \int_{t_{steady}}^T v_o(t) dt, \tag{14}$$

where  $t_{steady}$  is the starting point of the charging steady state and  $T$  is the total examined time of the output signal. The output DC power  $P_{DC}$  equals  $\frac{V_{DC}^2}{R}$ .

To compare the performance of different waveforms and equalization strategies, we define the normalized PCE as the harvested DC power divided by the transmitted power:

$$PCE_{norm} = \frac{P_{DC}}{\sum_{n=1}^{N_t} P_n}. \tag{15}$$

with  $P_n$  the power level of  $n$ -th tone.

To show how the PAPR and power level of the received signal influence the PCE of the rectifier, we simulate the DC output power of the half-wave rectifier using signals of varying PAPR at different power levels. We consider that the rectifier consists of a HSMS2850 Schottky diode, 150 pF load capacitor, 10 kΩ load resistor, and an optimized input matching network ensuring the full received RF signal goes through the rectifier. As the received signal, we consider two-tone multisine signals at different power levels and varying PAPR. We vary the amplitude ratio between the two tones  $\frac{|x_1|}{|x_2|}$  to ensure the same received power,  $P_r = \frac{|x_1|^2 + |x_2|^2}{2}$ , when considering multisine signals with PAPR varying from 2 to 4.

Figure 4 depicts the simulated DC output power and PCE of the rectifier with increasing PAPR of the received signals for different input power levels. It is shown that both  $P_{DC}$  and hence PCE increase with increasing PAPR for the same received power level. As expected, a higher received power results in more DC output power given the same PAPR of the signal. Since the ODE solver gives similar output when the input signal waveforms are similar, there exists some fluctuations in the range of PAPR between 2 and 2.3.

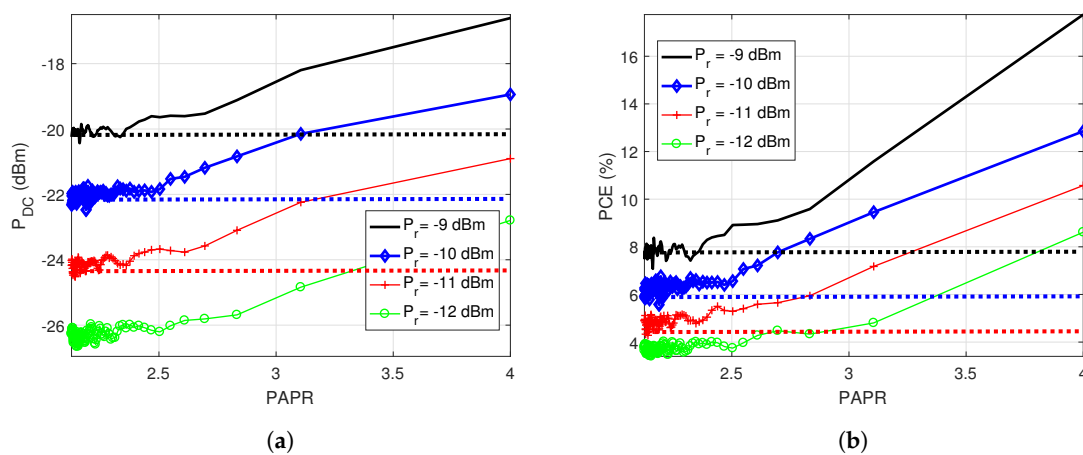


**Figure 4.** Simulated (a) direct current (DC) output power ( $P_{DC}$ ) and (b) power conversion efficiency (PCE) as a function of signal's PAPR at different received power levels at the receiver; the dotted lines of the same color plot the corresponding  $P_{DC}$  and PCE using CW (continuous-wave) excitation.

It is observed that, for a given  $P_r$ , PAPR has a significant impact on both  $P_{DC}$  and PCE. The dotted lines represent the DC output power and PCE using CW excitation at the same power levels. We can observe that for the given input power of  $-12$  dBm, a signal with maximal PAPR, four in this scenario, results in 3 dB more harvested power compared to the CW signal. Signals with PAPR larger than 3.2 can convert up to 1 dB more DC power even with 1 dB less received power, compared to the CW

signal, as Figure 4a shows. Moreover, the PCE is enhanced significantly (up to 9%) by using a signal of PAPR higher than four, as can be seen in Figure 4b. Even when the received power is 3 dB less than the power of the CW waveform, the signal with PAPR equal to 4 improves the PCE by 25%.

Measurements are performed to confirm the simulation results. The measurement set-up is depicted in Figure 5a. The vector signal transceiver (VST) PXIe-5645R from National Instruments is used to generate signals of different PAPR and input power levels that are applied to the rectifier. multisine signals of PAPR equal to 2, 4, 6, and 8 at different power levels are generated by tuning the number of tones from 1 to 4, and are then applied to the rectifier under test.

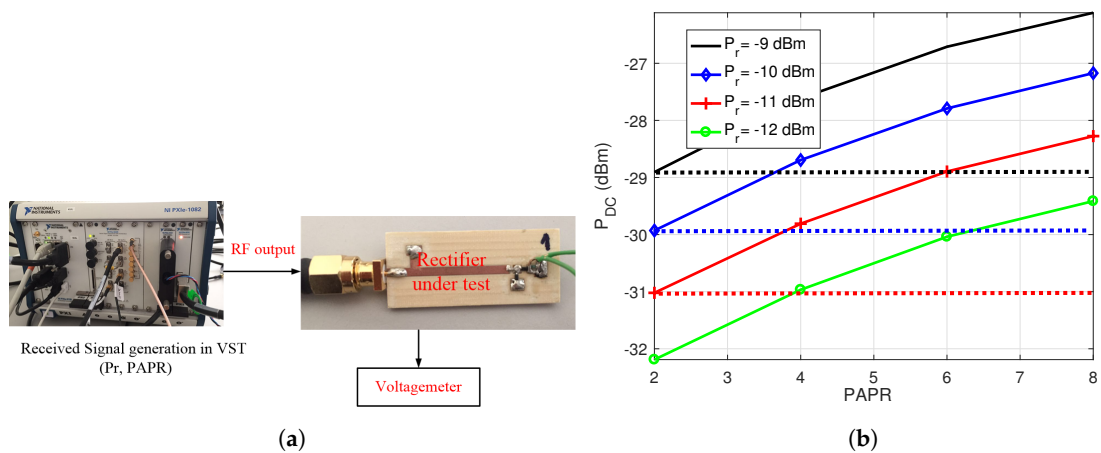


**Figure 5.** (a) Measurement set-up and (b) measured DC output power  $P_{DC}$  with increasing PAPR of the signal at different power levels; the dotted lines of the same color plot the corresponding  $P_{DC}$  using CW signal excitation.

It is observed in Figure 5b that the signals having a PAPR of 4 and 1 dB less received power improve the DC output power up to 1 dB, which corresponds to the simulation results. The measured DC power is less than the simulation results in Figure 4 since the rectifier's matching network is not perfect in reality. It is proven by measurements that with lower input power level within 1 dB difference, a higher PAPR signal could be converted to more DC power compared to the CW waveform, not to mention the benefits of improving the rectifier's PCE.

## 5. PAPR-Aware Transmission Strategies

In prior sections, we introduced the capacity of a multisine signal for the scenarios with and without amplitude modulation, and we also discussed that PAPR is important to optimize the PCE of a non-linear rectifier. In this section, we will introduce various pre-equalization strategies that optimize SNR or PAPR, or both. A PAPR-aware pre-equalizer compensates the frequency-selective channel for the modulated multisine SWIPT system. A balanced pre-equalizer is proposed, trading-off between the SNR of each bin and PAPR of the received signal. In Section 6, these pre-equalizers will then be compared.

### 5.1. Influence of Wireless Channel on PAPR

In this subsection, the channel influence on the PAPR of the received signal without pre-equalization is discussed. Once we understand this influence, an optimal pre-equalizer that determines the weights of each tone in a multisine signal, as to optimize the normalized PCE at the receiver, can be designed. The PAPR is calculated considering the block fading channel where the channel coefficients stay the same during the considered time block.

When considering a constant amplitude and no equalization, the  $PAPR_r$  of (7) becomes

$$PAPR_r = \frac{\text{Max}(A(t))^2}{\|\mathbf{h}\|^2 \frac{a^2}{2}} \leq \frac{2 \|\mathbf{h}\|_1^2}{\|\mathbf{h}\|^2}, \tag{16}$$

where  $A(t)$  can be written as

$$\begin{aligned} A(t) &= a \sqrt{\sum_{n=1}^{N_t} |h_n|^2 + \sum_{i \neq j} 2 |h_i| |h_j| \cos(\varphi_i(t) - \varphi_j(t))}, \\ &\leq a \|\mathbf{h}\|_1. \end{aligned} \tag{17}$$

The maximum PAPR is only reached when

$$\begin{aligned} \varphi_i(t) - \varphi_j(t) &= 2\pi(i - j)\Delta ft + \angle h_i - \angle h_j, \\ &= 0, \text{ for all } i \neq j, \end{aligned} \tag{18}$$

which means that all tones have the same phase at the receiver.

In addition to a phase constraint, there is an amplitude constraint. Given the fact that  $(N_t \|\mathbf{h}\|^2 - \|\mathbf{h}\|_1^2) = \sum_{i \neq j} (|h_i| - |h_j|)^2 \geq 0$ , we know that  $N_t \|\mathbf{h}\|^2 \geq \|\mathbf{h}\|_1^2$  or  $N_t \geq \frac{\|\mathbf{h}\|_1^2}{\|\mathbf{h}\|^2}$ . Then the PAPR, which is the ratio  $\frac{2\|\mathbf{h}\|_1^2}{\|\mathbf{h}\|^2}$  is always smaller than  $2N_t$  and reaches the maximum when  $|h_i| = |h_j|$ . Considering a frequency flat channel where each tone has the same channel coefficient  $h$ , PAPR is maximum and equal to  $2N_t$ , because the same channel implies  $|h_i| = |h_j|$  and  $\angle h_i = \angle h_j, i \neq j$ .

### 5.2. Pre-Equalization for Multisine PSK Modulation

To compensate the signal distortion caused by the frequency-selective channel, a pre-equalizer is introduced. The envelope of the pre-equalized signal when applying multisine PSK is

$$A_w(t) \leq a \|\mathbf{h} \circ \mathbf{w}\|_1 \text{ if } \varphi_i(t) - \varphi_j(t) = 0. \tag{19}$$

Thus the received signal PAPR is

$$PAPR_w \leq \frac{2 \|\mathbf{h} \circ \mathbf{w}\|_1^2}{\|\mathbf{h} \circ \mathbf{w}\|^2}. \tag{20}$$

The PAPR of the received pre-equalized signal reaches its maximum when  $|h_i| |w_i| = |h_j| |w_j|$  and  $\angle w_n = -\angle h_n$ . Without changing the transmit power,  $\|\mathbf{w}\|^2 = N_t$ , we can derive  $\mathbf{w}_{PAPR}$  as the element-wise inverse of the channel

$$\mathbf{w}_{PAPR} \propto \hat{\mathbf{h}}, \tag{21}$$

with  $\hat{\mathbf{h}} = \mathbf{h} \circ^{-1}$  and normalizing constant  $\sqrt{\frac{N_t}{\|\hat{\mathbf{h}}\|^2}}$  multiplied to  $\hat{\mathbf{h}}$ .

Based on the Cauchy–Schwarz inequality, the SNR of each tone (8) reaches a maximum when  $w_n$  is proportional to the conjugate of the channel coefficient  $h_n$ , namely matched pre-equalization. Ensuring that transmit power does not change, the matched pre-equalizer is

$$\mathbf{w}_m \propto \mathbf{h}^*, \tag{22}$$

with normalisation constant  $\sqrt{\frac{N_t}{\|\mathbf{h}\|^2}}$ .

Since the choice of the pre-equalizer influences both the PAPR and power level of the received signal, the crux of designing the transmission strategy for more converted DC power is whether the PAPR or the power level of the received signal impacts the DC output power the most.

A high PAPR signal indeed improves the PCE of the rectifier, yet a signal of lower power not only decreases the RF power that can be received by the rectifier, but also the PCE of the rectifier as addressed in Section 4.

To achieve as high as possible DC output, we propose a balanced pre-equalizer, ensuring the same transmit power, that is a linear combination of  $\mathbf{w}_{PAPR}$  and  $\mathbf{w}_m$ . This pre-equalizer is determined by two balancing coefficients  $(p, q)$  as below

$$\mathbf{w}_{bl} = p\mathbf{w}_{PAPR} + q\mathbf{w}_m, p \in [0, 1]. \quad (23)$$

The detailed computation of coefficients  $(p, q)$  is addressed in Appendix A ensuring no change in the transmit power. We denote the balanced pre-equalizer with coefficient  $p$  as  $\mathbf{w}_p$ . The optimal balancing coefficients are determined by a thorough search by computing the maximal DC power using the nonlinear power transfer model of this work. The computation time is around one hour. Potential relaxed solution to reduce the computation time can be studied in future work.

For comparison, the pre-equalizer achieving maximal channel capacity is also obtained. This pre-equalizer can be derived by solving the optimization problem as below

$$\begin{aligned} & \underset{\mathbf{w}_C}{\text{maximize}} C_{PSK} \quad (10) \\ & \text{subject to } \|\mathbf{w}_C\|^2 = N_t \end{aligned}$$

The solution of this optimization problem is

$$\mathbf{w}_C = \mathbf{1}, \quad (24)$$

which can be understood intuitively as the information is in the phase. The water-filling pre-equalizer to maximize the channel capacity is addressed in Appendix B.

Finally, we also compare our proposed pre-equalizers with the low-complexity transmission strategy for WPT proposed in [23] by which the pre-equalizer is proportional to  $|\mathbf{h}|^3 \angle \mathbf{h}^*$ .

Figure 6 plots the channel response of a two-tone multisine signal of 10 MHz, and the results of the considered pre-equalizers. It can be observed that the matched pre-equalizer assigns more power to the channel with higher gain, while the pre-equalizer maximizing the PAPR assigns more power to the channel with lower gain. For the balanced pre-equalizers, a moderate choice is made between the two extreme pre-equalizers depending on the choice of the balancing coefficients. Besides, the water filling pre-equalizer assigns the same amount of power to each bin, while the pre-equalizer  $w_{|\mathbf{h}|^3 \angle \mathbf{h}^*}$  boosts most of the power to the good channel.

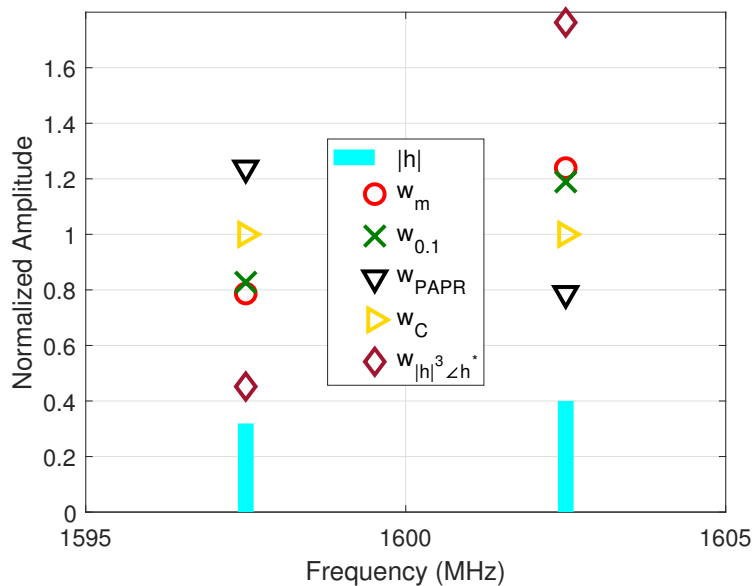


**Figure 6.** Normalized channel response amplitude and results of pre-equalizers  $w_m$ ,  $w_{PAPR}$ ,  $w_C$ ,  $w_{|h|^3 \angle h^*}$  and balanced pre-equalizer with  $p = 0.1$ , for a SWIPT system using two-tone multisine signals of 10 MHz.

### 5.3. Pre-Equalization for QAM Modulation

In this subsection, pre-equalizers for a QAM SWIPT system are addressed as a baseline to evaluate the corresponding pre-equalizers with the proposed multisine PSK SWIPT system.

Based on (6), the envelope of the received signal applying complex normal symbol input is

$$A_{QAM}(t) \leq \|x \circ h \circ w\|_1. \tag{25}$$

Since  $\phi_n$  is a random value, the phase difference  $[\varphi_i(t) - \varphi_j(t)] = 2\pi(i - j)\Delta ft + \phi_i - \phi_j$  has a small probability to achieve zero for all  $n$  at the same time even ensuring  $\angle w_n = -\angle h_n$ . Thus, the PAPR of the signal is a lot smaller than the bound  $\frac{\|x \circ h \circ w\|_2^2}{\|x \circ h \circ w\|_1^2}$ . The maximum PAPR upper-bound is achieved when  $|x_i||h_i||w_i| = |x_j||h_j||w_j|$ . While the pre-equalizer  $w_{PAPR}$  can compensate the channel  $h$ , the symbol amplitude variations cannot be compensated so it is unlikely that the multi-tone QAM signal reaches the peak PAPR  $2N_t$ .

The corresponding matched pre-equalizer and balanced pre-equalizer are the same as the ones for multisine PSK based SWIPT system.

However, the pre-equalizer maximizing the QAM capacity is a water-filling scheme as  $w_{n,C} = \sqrt{\left(v - \frac{z}{|h_n|^2}\right)^+} \angle h_n^*$  with  $v = 1 + \frac{(1-\rho)\sigma^2 + \sigma_{\text{mixer}}^2}{(1-\rho)P_t} \|\hat{h}\|^2$ ,  $z = \frac{[(1-\rho)\sigma^2 + \sigma_{\text{mixer}}^2]N_t}{(1-\rho)P_t}$ .

## 6. Results

We simulate the SWIPT performance with an eight-tone multisine signal of transmit power  $-10$  dBm, that experiences a Rayleigh fading frequency-selective channel of normalized channel gain one. The noise figure is 10 dB in both channel and mixer. We apply the various pre-equalizers considered in previous section, and analyse the results.

### 6.1. Information Rate Comparison

Figure 7 depicts the capacity of the multisine SWIPT system with increasing power splitting factor  $\rho$  for multisine PSK modulation and QAM modulation with complex normal symbol input. The channel capacity decreases with increasing  $\rho$  since more power goes into the rectifier. For both

cases the pre-equalizer maximizing the capacity leads to the highest channel capacity, as expected. The pre-equalizer designed to optimize the harvested power in [23] leads to the lowest channel capacity for both modulation schemes because the channels that are not good enough for power transfer are not sufficiently exploited for information transfer. The balanced pre-equalizers, however, provide fair performance regarding the channel capacity. We see that the capacity applying multisine PSK modulation equals around half of the capacity applying complex normal symbol input, since only the phase is modulated but not the amplitude and therefore one degree of modulation freedom is lost. In the remainder of this paper, we will focus on a high  $\rho = 0.9$ , unless stated otherwise, as this achieves a relatively high capacity and it will maximize power conversion efficiency.

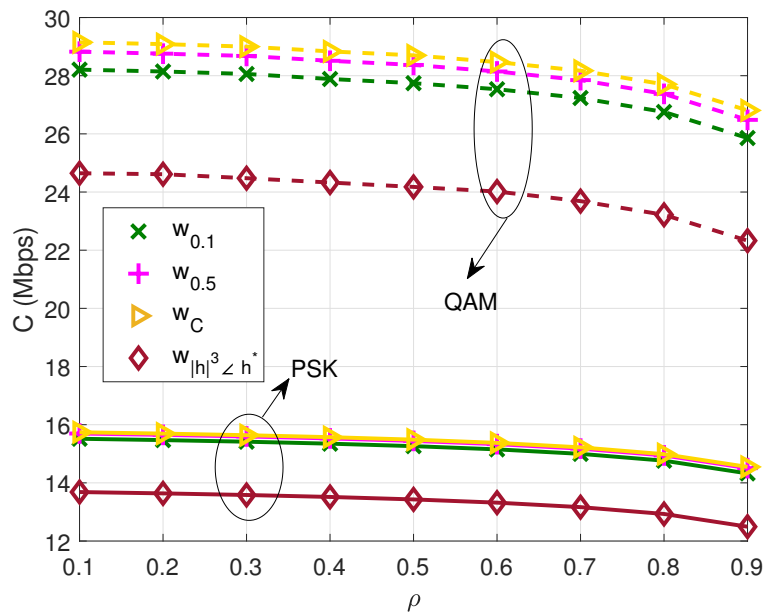


Figure 7. Capacity as a function of  $\rho$  for an 8-tone signal using multisine PSK and QAM modulation of 1 MHz BW, and adopting the proposed pre-equalisers.

### 6.2. PCE Measurement and Simulation Results

To validate our PCE model, we measured the normalized PCE of the multisine PSK modulated SWIPT system with increasing BW using the circuit in Figure 5a, applying the proposed pre-equalizers. Simulations with the same circuit parameters are also performed.

Figure 8 plots the normalized PCE of the SWIPT system with increasing BW using an eight-tone multisine signal when the power splitter coefficient is 0.9. In both simulations and measurements, the balanced pre-equalizer  $p = 0.1$  and the matched filter achieve the highest normalized PCE. Besides, the matched pre-equalizer performs very close to  $w_{0.1}$ . In addition, the pre-equalizer maximizing the PAPR gives the lowest normalized PCE. Nevertheless, in the measurements, the PCE using the pre-equalizer maximizing the PAPR is not so low as in the simulation. This is because the diode performs even more nonlinearly with increasing voltage than the Shockley equation describes and also the parasitic effects are not taken into account. It should be noted that in Figure 8, the normalized PCE can be as high as 80% which approaches the optimal theoretical PCE. This phenomenon actually shows the fact that normalized PCE can be improved by exploiting channel diversity.

To clarify why the balanced pre-equalizer has the best performance on WPT, we further analyze the impact of received power and PAPR. The power levels of the received signals with increasing  $\rho$  using different pre-equalizers are plotted in Figure 9. As the pre-equalization is the same for both modulations, and each modulation has the same signal power, the received powers are the same for both multisine PSK and QAM modulations. The final PAPR of the received signals using multisine PSK is plotted at the left side of Figure 10. It is shown that the balanced pre-equalizer of  $p = 0.1$  and

the matched pre-equalizer have a similar PAPR and received power. The pre-equalizer  $w_{PAPR}$  gives the highest PAPR and lowest received power; while the  $w_{|h|^3 \angle h^*}$  gives the lowest PAPR and highest received power; both of them provide sub-optimal SWIPT performance.

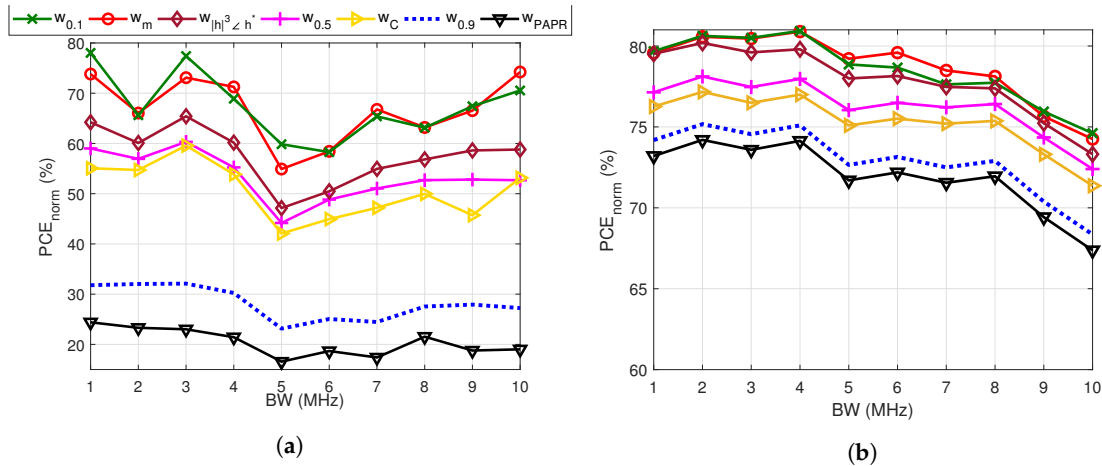


Figure 8. (a) Simulated and (b) measured normalized PCE with increasing BW using the proposed pre-equalizers of a two-tone based SWIPT system with  $\rho = 0.9$ .

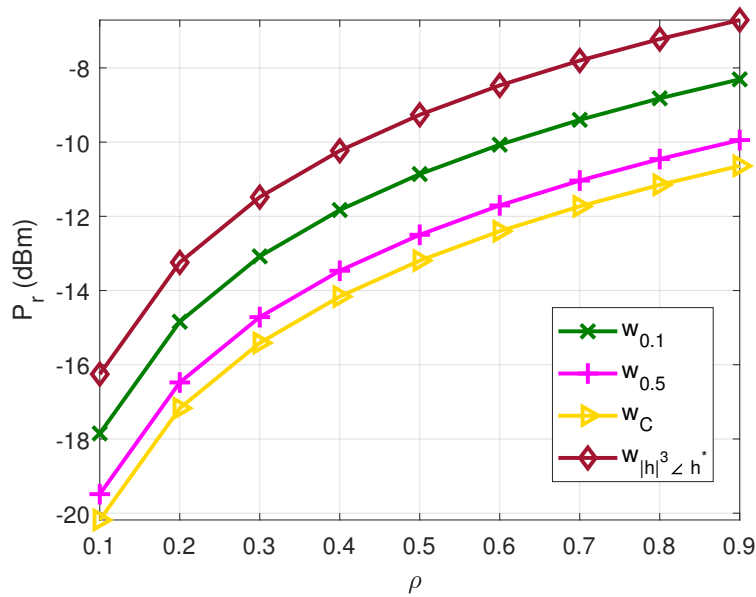
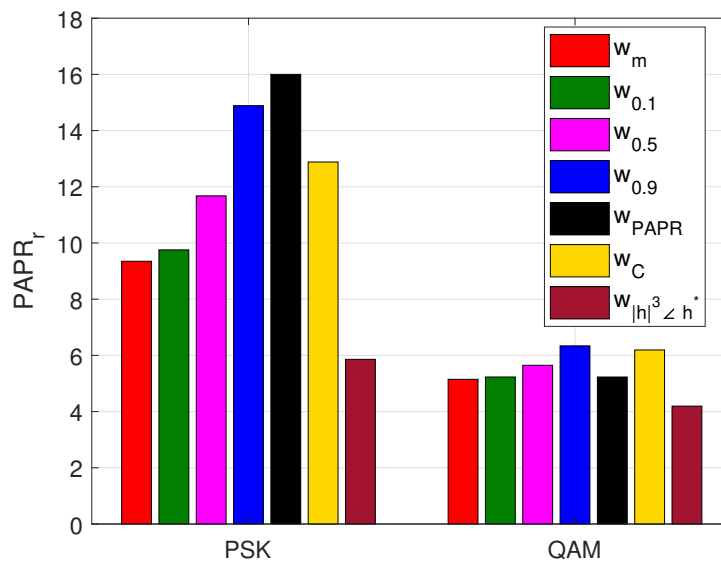


Figure 9. Received power  $P_r$  as a function of the splitting coefficient  $\rho$  using the proposed pre-equalizers in an 8-tone signal based SWIPT system of bandwidth 1 MHz.



**Figure 10.** PAPR of the received signals using multisine PSK modulation and QAM modulation using the proposed pre-equalizers of an 8-tone based SWIPT of bandwidth 1 MHz.

### 6.3. Information and Power Trade-off

From the previous results, it is shown that the balanced pre-equalizer with  $p = 0.1$  provides the maximal normalized PCE for multisine PSK modulated SWIPT and the balanced pre-equalizer with  $p = 0.5$  provides capacity approaching the maximum value for both modulation schemes. In this subsection, we further compare the SWIPT performance of the proposed multisine PSK modulation with the QAM-OFDM scheme, by investigating the trade-off between information and power transfer. We apply the balanced pre-equalizer with  $p = 0.1, 0.5$ . The proposed WPT pre-equalizer from [23] and the pre-equalizer maximizing capacity are also considered as a baseline for evaluating performance of power and information transfer.

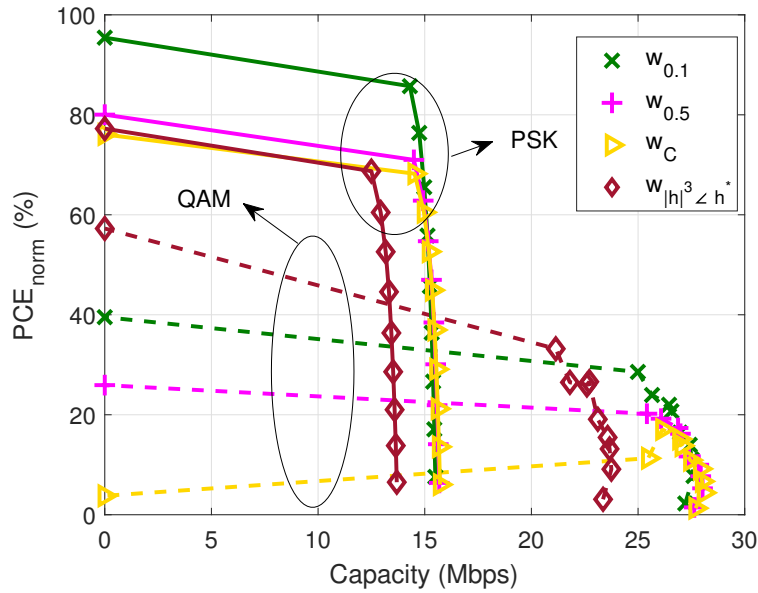
Figure 11 shows the normalized PCE-capacity boundary when varying the power splitting factor from 0.1 to 1. The multisine based SWIPT experiences a frequency-selective channel with normalized gain one. It is shown for the multisine PSK based SWIPT that the balanced equalizer with  $p = 0.1$  leads to the largest PCE-capacity region, while the pre-equalizer  $w_{|h|^3 < h^*}$  [23] leads to the smallest region. Nevertheless, for QAM based SWIPT, the pre-equalizer  $w_{|h|^3 < h^*}$  provides the highest normalized PCE and  $w_C$  still provides the lowest PCE and the highest capacity. It is noted that when the power-splitting factor is higher than 0.9, the water-filling algorithm tends to allocate no power to the bad channels which also lowers the power transfer performance. In addition, by comparing the two modulation schemes, it is shown the maximum normalized PCE improves up to 140% by applying multisine PSK when the power splitting coefficient is 1.

As can be seen from Figure 9, the received power achieves the highest value by using pre-equalizer  $w_{|h|^3 < h^*}$  compared to the other pre-equalizers. Besides, as expected, the PAPR of the signal applying complex normal symbol input is much lower than the PAPR of the signal applying the multisine PSK scheme, as can be seen in Figure 10.

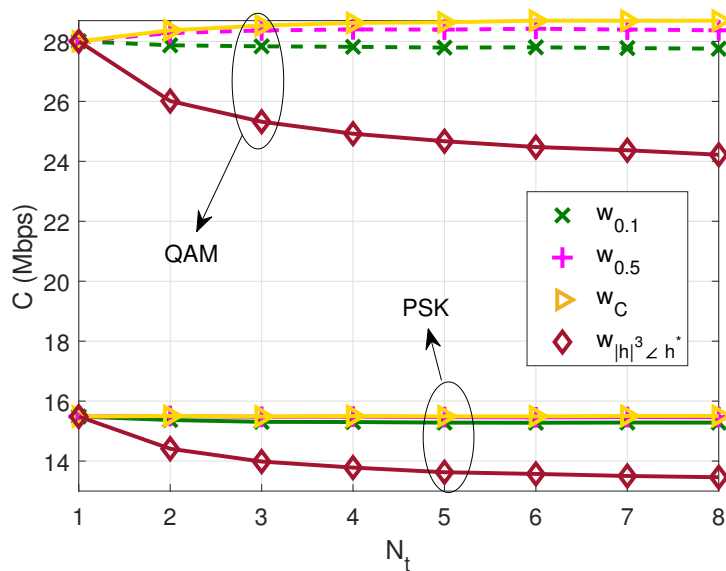
To give more insight in the interplay between the wireless channel and the modulation strategy, we further discuss the impact of the number of tones on the SWIPT performance for multisine PSK and QAM.

Figure 12 shows the capacity with increasing number of tones in the multisine based SWIPT when applying multisine PSK modulation and complex normal input symbols at fixed BW. It is shown that the capacity is almost flat with increasing number of tones when the balanced pre-equalizers are applied in the multisine PSK SWIPT. This is because when the signal BW is fixed, the total capacity

$C \simeq B \log_2\left(\frac{4\pi}{e} \frac{P_f}{N_f}\right)$  which mainly depends on the variance of  $\log_2\left(\frac{4\pi}{e} \frac{P_f}{N_f}\right)$  that only decreases in a small range with increasing  $N_f$ . The pre-equalizer  $\mathbf{w}_{|h|^3/h^*}$  assigns major power to the good sub-channels and loses the information in the other sub-channels. In addition, for QAM modulation, more capacity is gained when it is possible to exploit the channel statistics and apply water-filling, but this improvement saturates when the number of tones is large enough since the SNR of each sub-channel also decreases.



**Figure 11.** Normalized PCE-capacity boundary using multisine PSK modulation and QAM for  $\rho$  ranging from 0.1 to 1 for 8-tone multisine signal of 1 MHz BW.



**Figure 12.** Capacity using multisine PSK modulation and QAM modulation with increasing number of tones, with  $\rho = 0.5$  and  $B = 1$  MHz.

The normalized PCE increases with the number of tones as shown in Figure 13. Looking at Figure 15, it is shown that the balanced pre-equalizers  $p = 0.1, p = 0.5$ , and  $\mathbf{w}_{|h|^3/h^*}$  improve the received power with increasing number of tones, while the pre-equalizer  $\mathbf{w}_{maxC}$  results in a slightly decreased power with increasing number of tones. However, the pre-equalizers that decrease the received power improve the received signal PAPR significantly, as shown in Figure 14, which results

in an improvement of normalized PCE. For the QAM modulated SWIPT system, the pre-equalizer  $w_{|h|^3 \angle h^*}$  leads to the highest normalized PCE. This is because the PAPR improvement by using balanced pre-equalizers is too small to compensate the received power loss up to 7 dB, as can be seen in Figures 14 and 15. Overall, the maximum normalized PCE using the QAM-OFDM modulation is about 50% less than that using the multisine PSK scheme since the PAPR using QAM is much lower than the one using multisine PSK.

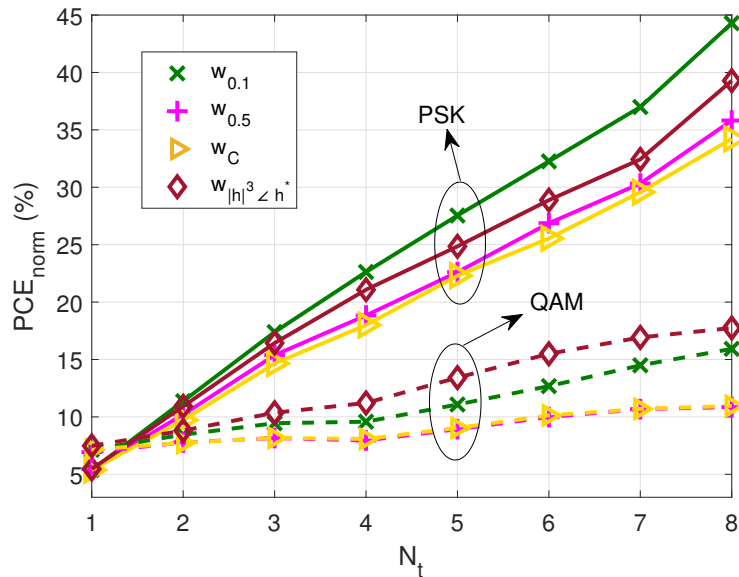


Figure 13. Normalized PCE using multisine PSK modulation and QAM modulation as a function of  $N_t$  for multisine based SWIPT system with  $\rho = 0.5$  and  $B = 1$  MHz.

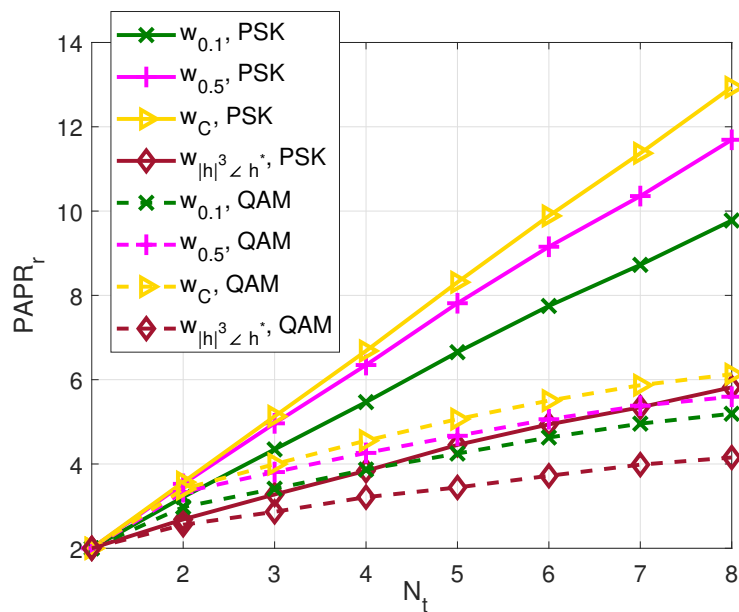
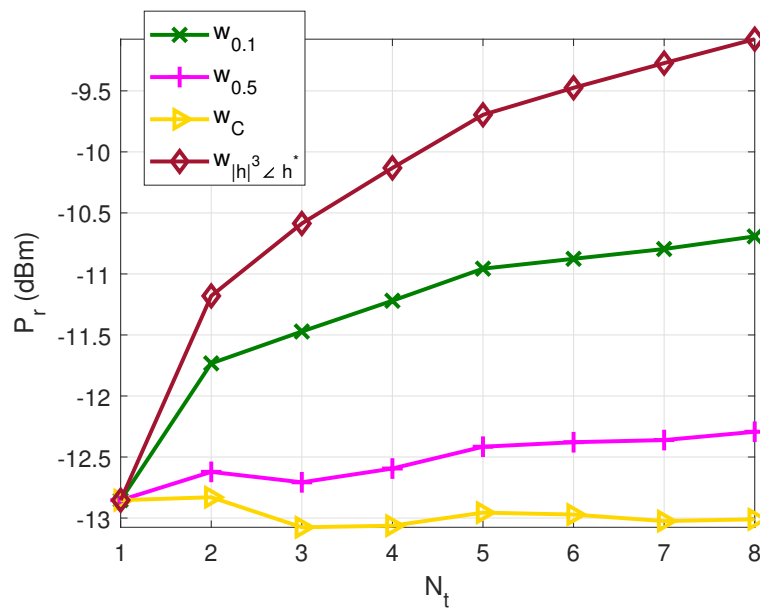


Figure 14. PAPR of received signals using multisine PSK modulation and QAM modulation- to explain symbol on y-axis better. with increasing  $N_t$  using the proposed pre-equalizers of a multisine SWIPT system.



**Figure 15.** Received power as a function of the number of tones using the proposed pre-equalizers in a multisine SWIPT,  $\rho = 0.5$ ,  $B = 1$  MHz.

## 7. Conclusions

In this paper, we propose a multisine PSK modulation and pre-equalization strategies to optimize the PCE for a SWIPT system with a realistic rectifier model. Compared to the state-of-the-art SWIPT systems, focusing on both amplitude and phase modulation, we show that our strategy improves PCE by more than a factor of two, at the cost of a lower spectral efficiency.

This conclusion is based on a broad comparison of multiple pre-equalization strategies, verified using measurements. The main insights derived from the study is that PAPR is very important to optimize PCE, exploiting the rectifier non-linearity. The proposed transmission strategy, including a pre-equalization and modulation technique that boosts the PAPR, is hence able to achieve the maximum PCE. On the other hand, when the PAPR optimization is not considered, e.g., because of amplitude modulation or when using a simplified rectifier model, our analysis shows that boosting the sub-carrier with the best channel is optimal in terms of the power and capacity trade-off.

We also show that the use of multiple tones can significantly improve PCE, while the impact on capacity is rather small and only when doing optimal water-filling. When using multisine PSK modulation, capacity is not improved when using multiple tones.

We propose a practical balanced pre-equalizer that can balance the benefits of PAPR and received power optimization for multisine PSK modulation. Based on an empirical weighing factor  $p = 0.1$ , we can achieve the largest power-rate trade-off region for multisine PSK and for the rectifier we considered. A comparison for other rectifier models, or an analysis on how to determine the best balancing factor remains for future work.

**Author Contributions:** Conceptualization, N.P. and S.P.; methodology, N.P., M.R., S.C., D.S. and S.P.; software, N.P.; validation, N.P., M.R. and S.C.; formal analysis, N.P.; investigation, N.P., M.R. and S.C.; data curation, N.P.; writing—original draft preparation, N.P.; writing—review and editing, S.C., D.S. and S.P.; visualization, N.P.; supervision, D.S. and S.P. All authors have read and agreed to the published version of the manuscript.

**Funding:** This research was funded by FWO-Flanders (Fonds voor Wetenschappelijk Onderzoek-Vlaanderen) and Hercules.

**Acknowledgments:** The authors acknowledge Daniel Belo from the University of Aveiro, Portugal for constructing the rectifier under test.

**Conflicts of Interest:** The authors declare no conflict of interest.

## Appendix A

In this Appendix, we describe the detailed process to determine the balancing coefficients  $(p, q)$ .

Ensuring transmit power does not change  $\|\mathbf{w}\|^2 = N_t$ , we can derive the relation between the balanced coefficients as

$$p^2 + q^2 + \frac{2pqN_t}{\sqrt{\|\hat{\mathbf{h}}\|^2 \|\mathbf{h}\|^2}} = 1. \quad (\text{A1})$$

The coefficient  $p$  is chosen from 0 to 1. Then the coefficient  $q$  can be computed following the equation below

$$q = \sqrt{1 - p^2 + p^2 c^2} - pc, \quad c = \frac{N_t}{\sqrt{\|\hat{\mathbf{h}}\|^2 \|\mathbf{h}\|^2}} \quad (\text{A2})$$

## Appendix B

The water-filling pre-equalizer to maximize the channel capacity is addressed in this appendix. Since  $|x| = a$ , the maximization problem (24) is simplified as

$$\begin{aligned} & \underset{w_n}{\text{maximize}} && \sum_{n=1}^{N_t} \log_2 \left( \frac{4\pi T_s (1-\rho) |h_n w_n|^2 \frac{a^2}{2}}{e (1-\rho) \sigma^2 + \sigma_{mixer}^2} \right) \\ & \text{subject to} && \sum_{n=1}^{N_t} |w_n|^2 = N_t. \end{aligned} \quad (\text{A3})$$

The Lagrange function is

$$\begin{aligned} \mathcal{L}(w_n) = & \sum_{n=1}^{N_t} \log_2 \left( \frac{4\pi (1-\rho) |h_n w_n|^2 \frac{a^2}{2}}{e (1-\rho) \sigma^2 + \sigma_{mixer}^2} \right) \\ & - \lambda \left( \sum_{n=1}^{N_t} |w_n|^2 - N_t \right). \end{aligned} \quad (\text{A4})$$

Based on the Karush–Kuhn–Tucker (KKT) conditions that

$$\nabla \mathcal{L}(w_n) = \frac{1}{\ln 2} \frac{e [(1-\rho)\sigma^2 + \sigma_{mixer}^2]}{w_n} - \lambda w_n^* = 0, \quad (\text{A5a})$$

$$\lambda \left( \sum_{n=1}^{N_t} |w_n|^2 - N_t \right) = 0, \quad (\text{A5b})$$

the optimal pre-equalizer is  $w_{n,C} = 1$ .

## References

1. Bi, S.; Zeng, Y.; Zhang, R. Wireless Powered Communication Networks: An Overview. *IEEE Wirel. Commun.* **2016**, *23*, 10–18. [\[CrossRef\]](#)
2. Clerckx, B.; Costanzo, A.; Georgiadis, A.; Carvalho, N.B. Toward 1G Mobile Power Networks: RF, Signal, and System Designs to Make Smart Objects Autonomous. *IEEE Microw. Mag.* **2018**, *19*, 69–82. [\[CrossRef\]](#)
3. Boaventura, A.; Collado, A.; Georgiadis, A.; Carvalho, N. Spatial Power Combining of Multi-Sine Signals for Wireless Power Transmission Applications. *IEEE Trans. Microw. Theory Tech.* **2014**, *62*, 1022–1030. [\[CrossRef\]](#)
4. Collado, A.; Georgiadis, A. Optimal Waveforms for Efficient Wireless Power Transmission. *IEEE Microw. Compon. Lett.* **2014**, *24*, 354–356. [\[CrossRef\]](#)
5. Pan, N.; Boaventura, A.S.; Rajabi, M.; Schreurs, D.; Carvalho, N.B.; Pollin, S. Amplitude and Frequency Analysis of Multi-sine Wireless Power Transfer. In Proceedings of the 2015 IEEE Int. Workshop on Integrated Nonlinear Microwave and Millimetre-Wave Circuits, Taormina, Italy, 1–2 October 2015; pp. 1–3.

6. Rajabi, M.; Pan, N.; Pollin, S.; Schreurs, D. Impact of Multisine Excitation Design on Rectifier Performance. In Proceedings of the 46th European Microwave Conference, London, UK, 3–7 October 2016; pp. 1151–1154.
7. Shi, Q.; Liu, L.; Xu, W.; Zhang, R. Joint Transmit Beamforming and Receive Power Splitting for MISO SWIPT Systems. *IEEE Trans. Wirel. Commun.* **2014**, *13*, 3269–3280. [[CrossRef](#)]
8. Wang, F.; Peng, T.; Huang, Y.; Wang, X. Robust Transceiver Optimization for Power-Splitting Based Downlink MISO SWIPT Systems. *IEEE Signal Process. Lett.* **2015**, *22*, 1492–1496. [[CrossRef](#)]
9. Shi, Q.; Peng, C.; Xu, W.; Hong, M.; Cai, Y. Energy Efficiency Optimization for MISO SWIPT Systems With Zero-Forcing Beamforming. *IEEE Trans. Signal Process.* **2016**, *64*, 842–854. [[CrossRef](#)]
10. Dong, Y.; Ge, X.; Hossain, M.J.; Cheng, J.; Leung, V.C.M. Proportional Fairness-Based Beamforming and Signal Splitting for MISO-SWIPT Systems. *IEEE Commun. Lett.* **2017**, *21*, 1135–1138. [[CrossRef](#)]
11. Boshkovska, E.; Ng, D.W.K.; Zlatanov, N.; Schober, R. Practical Non-Linear Energy Harvesting Model and Resource Allocation for SWIPT Systems. *IEEE Commun. Lett.* **2015**, *19*, 2082–2085. [[CrossRef](#)]
12. Boshkovska, E.; Morsi, R.; Ng, D.W.K.; Schober, R. Power Allocation and Scheduling for SWIPT Systems with Non-linear Energy Harvesting Model. In Proceedings of the IEEE International Conference on Communication, Kuala Lumpur, Malaysia, 23–27 May 2016; pp. 1–6.
13. Clerckx, B.; Bayguzina, E. Waveform Design for Wireless Power Transfer. *IEEE Trans. Signal Process.* **2016**, *64*, 6313–6328. [[CrossRef](#)]
14. Zeng, Y.; Clerckx, B.; Zhang, R. Communications and Signals Design for Wireless Power Transmission. *IEEE Trans. Commun.* **2017**, *65*, 2264–2290. [[CrossRef](#)]
15. Xu, X.; Ozcelikkale, A.; McKelvey, T.; Viberg, M. Simultaneous Information and Power Transfer under a Non-Linear RF Energy Harvesting Model. In Proceedings of the IEEE International Conference on Communication Workshops, Paris, France, 21–25 May 2017; pp. 179–184.
16. Pan, N.; Claessens, S.; Rajabi, M.; Pollin, S.; Schreurs, D. Discussion on Rectifier Models for Wireless Power Transfer Excitation Design. In Proceedings of the IEEE Asia-Pacific Microwave Conference, Singapore, 10–13 December 2019; pp. 1–3.
17. Pan, N.; Belo, D.; Rajabi, M.; Schreurs, D.; Carvalho, N.B.; Pollin, S. Bandwidth Analysis of RF-DC Converters Under Multisine Excitation. *IEEE Trans. Microw. Theory Tech.* **2018**, *66*, 791–802. [[CrossRef](#)]
18. Morsi, R.; Jamali, V.; Ng, D.W.K.; Schober, R. On the Capacity of SWIPT Systems with a Nonlinear Energy Harvesting Circuit. *arXiv* **2017**, arXiv:1711.01082.
19. Varasteh, M.; Rassouli, B.; Clerckx, B. On Capacity-Achieving Distributions Over Complex AWGN Channels Under Nonlinear Power Constraints and their Applications to SWIPT. *arXiv* **2017**, arXiv:1712.01226.
20. Bayguzina, E.; Clerckx, B. Modulation Design for Wireless Information and Power Transfer with Nonlinear Energy Harvester Modeling. In Proceedings of the IEEE International Workshop on Signal Processing Advances in Wireless Communications, Kalamata, Greece, 25–28 June 2018; pp. 1–5.
21. Claessens, S.; Pan, N.; Rajabi, M.; Schreurs, D.; Pollin, S. Enhanced Biased ASK Modulation Performance for SWIPT With AWGN Channel and Dual-Purpose Hardware. *IEEE Trans. Microw. Theory Tech.* **2018**, *66*, 3478–3486. [[CrossRef](#)]
22. Rajabi, M.; Pan, N.; Claessens, S.; Pollin, S.; Schreurs, D. Modulation Techniques for Simultaneous Wireless Information and Power Transfer With an Integrated Rectifier–Receiver. *IEEE Trans. Microw. Theory Tech.* **2018**, *66*, 2373–2385. [[CrossRef](#)]
23. Clerckx, B.; Bayguzina, E. Low-Complexity Adaptive Multisine Waveform Design for Wireless Power Transfer. *IEEE Antennas Wirel. Propag. Lett.* **2017**, *16*, 2207–2217. [[CrossRef](#)]
24. Reams, R. Hadamard inverses, square roots and products of almost semidefinite matrices. *Linear Algebra Appl.* **1999**, *288*, 35–43. [[CrossRef](#)]
25. Tse, D.; Viswanath, P. *Fundamentals of Wireless Communication*; Cambridge University Press: Cambridge, UK, 2005.
26. Moskowitz, M.A. *A Course in Complex Analysis in One Variable*; World Scientific: Singapore, 2002.

27. Valenta, C.; Durgin, G. Rectenna Performance Under Power-optimized Waveform Excitation. In Proceedings of the IEEE Int. Conf. on RFID, Orlando, FL, USA, 30 April–2 May 2013; pp. 237–244.
28. E. Blahut, R. *Principles and Practice of Information Theory*; Addison-Wesley Publishing Company: Boston, MA, USA, 1987.



© 2020 by the authors. Licensee MDPI, Basel, Switzerland. This article is an open access article distributed under the terms and conditions of the Creative Commons Attribution (CC BY) license (<http://creativecommons.org/licenses/by/4.0/>).